Available online at www.sciencedirect.com
SCIENCE DIRECT
International Journal of Thermal Sciences 45 (2006) 796–803
International Journal of Thermal Sciences
www.elsevier.com/locate/ijts

Interfacial energies of aqueous mixtures and porous coverings for enhancing pool boiling heat transfer

Elva Meléndez [a], René Reyes [b,*]

[a] *CIICAp, Universidad Autónoma del Estado de Morelos, 62210, Mexico*
[b] *Departamento de Ingeniería Química y Alimentos, Universidad de las Américas Puebla, Santa Catarina Mártir Cholula, Puebla 72820, Mexico*

Received 28 June 2005; accepted 22 November 2005

Available online 10 January 2006

Abstract

The interfacial energies effects on pool boiling were measured for combinations of aqueous ethanol mixtures and cationic surfactants. The mixture with 16% ethanol by weight had the lowest contact angle (associated to the highest wettability) and produced the highest convective heat transfer coefficient, h, among the aqueous ethanol mixtures. The surfactant sodium–lauryl–sulfate added at 100 ppm (its calculated critical micelle concentration CMC) to the 16% ethanol aqueous mixture produced an additional increment of the wettability of the mixture and of the h values; other concentrations of the surfactant reduced de contact angle and h values. The effect of these interfacial energies represents a mass-transfer contribution to pool boiling and the proposal of mixture effects both as increased spreadibility and as micelle states. Several randomly constructed porous coverings, contributing to the breakage of vapor slugs around the heater, were tested; produced the highest h values for average pore diameters of 0.5 mm, and covering thickness of 0.972 mm. The synergistic effect on h of the interfacial energies of mixtures at their critical micelle concentration, and porous coverings was measured. Therefore, the independent driving forces combined in this study for increasing pool boiling heat transfer are (a) spreadibility of the liquid on the solid; (b) the bubble's size reduction, achieved by micelle states; and (c) the bubble's breakage, induced by the porous coverings, for vapor flow not under pressure drop control.

Keywords: Contact angle; Interfacial energies; Wettability; Porous coverings; Pool boiling

1. Introduction

1.1. Surface and interfacial energies and the sessile drop contact angle

Surface and interfacial energies express mass transfer effects on pool boiling at the heater–liquid or the liquid–vapor interfaces. Under proper conditions, the transport of minute concentrations of a surface active substance in a pure substance, or the lower vapor-pressure substance in a binary mixture, modifies the interfacial energy and the boiling characteristics significantly [1].

The surface or interfacial tension is a measurement of the imbalance of the cohesion energy on the molecules present at an interface. The molecules in the bulk of a liquid are attracted one to the other, and equal forces surrounding the molecules balance the interactions. Instead, the interface molecules are subjected to a force imbalance that provides them with free energy greater than to those in the bulk and causes interfacial surface area reduction. The terms normally applied to the free energy in the surface interface are interfacial energy or tension for liquid to fluid interfaces, and surface energy or tension for solid to fluid interfaces [2].

Several models have been proposed for the description of the surface and interfacial energies. Fowkes [3,4] formulated a model for the interfacial energy of phases 1 and 2 interacting through dispersion forces, D

$$\sigma_{12} = \sigma_1 + \sigma_2 - 2\sqrt{\sigma_1^D \sigma_2^D} \tag{1}$$

In Eq. (1) the interfacial tension, a thermodynamic property, is formulated as a mechanical property, the surface internal energy (U), and considered independent of temperature (T), because the Helmholtz energy for the surface ($U - TS$) was

* Corresponding author. Tel.: +52 222 229 2660; fax: +52 222 229 2727.
E-mail address: rreyes@mail.udlap.mx (R. Reyes).

1290-0729/$ – see front matter
doi:10.1016/j.ijthermalsci.2005.11.005

Nomenclature

h	convective heat transfer coefficient	$W\,m^{-2}\,K^{-1}$
C	coverings	
CHF	Critical Heat Flux condition	
d	diameter	mm
K	permeability	m^2
$\overset{\circ}{m}$	mass flow	$kg\,s^{-1}$
N	number of pores per unit surface area	
P	pressure	Pa
q	heat transfer	W
q''	heat flux	$W\,m^{-2}$
T	temperature	K
t	thickness	mm
S	total surface entropy	$mJ\,m^{-2}\,K^{-1}$
U	surface internal energy	$mJ\,m^{-2}$
V	vapor release velocity	$m\,s^{-1}$

Greek symbols

Δ	gradient or difference
ε	porosity
μ	viscosity — Pa s
π	spreading pressure — $mPa\,m^{-1}$
θ	equilibrium contact angle — degrees
ρ	density
σ	interfacial tension or surface free energy — $mJ\,m^{-2}$

Sub-fixes and super-fixes

a	associated to a surface
D	dispersion forces
l	liquid
P	non-dispersion or polar forces
p	pore
s	solid
v	vapor
1, 2	two phases or sequential numbering

related only to U excluding S. The work of adhesion, in this context, is formulated as a temperature independent geometric mean of the energies of the phases involved. Eq. (1) makes a good description of wetting and adhesion processes in conjunction with contact angles because the same type of approximation is made for two coupled phenomena, interfacial tension and contact angle [5,6].

Despite the conceptual limitations for the use of the geometric mean for dispersion, D, and the polar, P, components of the interfacial tension, the expression proposed by Fowkes [7] is also sufficient for analysis of wetting phenomena:

$$\sigma_{12} = \sigma_1 + \sigma_2 - 2\sqrt{\sigma_1^D \sigma_2^D} - 2\sqrt{\sigma_1^P \sigma_2^P} \tag{2}$$

The equation used for the calculation of surface or interfacial free energies results from the combination of Eq. (3) and Young's equation:

$$\sigma_{sv} - \sigma_{sl} = \sigma_{lv}\cos\theta + \pi \tag{3}$$

where σ_{sv} and σ_{sl} are the surface tensions of the solid/vapor and solid/liquid interfaces, respectively; σ_{lv} is the interfacial tension of the liquid/vapor interface; θ is the measured sessile drop contact angle; and π is the spreading pressure, the difference between the surface free energies of the solid–vacuum interface and the solid-saturated vapor interface, a term neglected in most textbooks. Eq. (3) relates the contact angle to surface and interfacial energies and to the wettability or spreadibility of the liquid on a solid surface. Low values of θ describe high wettability systems from the notion that "when the liquid wets the solid completely and spreads freely over the surface at a rate depending on the liquid viscosity and the solid surface roughness, we say that $\theta = 0\ldots$. Since the tendency for the liquid to spread increases as θ decreases, the contact angle is a useful inverse measure of spreadibility or wettability." We rely on the evaluation of the sessile drop contact angle for measuring the system's wettability because σ_{sv} and σ_{sl} cannot be conveniently and reliably measure [8].

The sessile drop contact angles could describe the state of cleanliness of the metallic surfaces by comparing the values obtained under similar measurement conditions. However, the calculation of the dispersion and polar components of the solid's surface energy is possible combining Eqs. (2) and (3) in a linear relationship [9]:

$$\frac{\sigma_{lv}(1+\cos\theta)}{2\sqrt{\sigma_l^D}} = \frac{\sigma_l^P \sigma_s^P}{\sigma_l^D} + \sqrt{\sigma_s^D} \tag{4}$$

to calculate σ_s^P and σ_s^D (then $\sigma_{ss} = \sigma_s^P + \sigma_s^D$) from a linear regression analysis using a set of probe liquids of known σ_{lv}, σ_l^D, and σ_l^P. The experimental error associated with the evaluation of σ_{ss} (conventionally related to σ_{sv} without further analysis) depends on the reliability of the interfacial tension data of the probe liquids and the measurement of the equilibrium contact angle. Conversely, it is possible to use Eq. (4) for the calculation of σ_l^D and σ_l^P with known values of σ_{lv}, σ_s^D and σ_s^P of a set of probe solids and liquids. Thus, an approximate measurement of surface and interfacial tensions is possible through the sessile-drop contact angle and known values of σ_{sv} and σ_{lv}. This study, proposes the modulation of surface and interfacial energies for increasing the boiling system wettability (observed through contact angle values) and the convective heat transfer coefficient h.

1.2. The Hamaker constant

Another approach for calculation of the interfacial phenomena acting in boiling considers the expression of intermolecular forces through a very thin adsorbed liquid layer at the contact line region [1,10]. The Hamaker constant describes the intermolecular interactions between the solid surface, the thin-film-

adsorbed liquid layer, and the vapor phase (disjoining pressure) at the contact line region of rewetting phenomena [11] and at a nucleation site cavity under critical heat flux conditions [10]. The evaluation of the Hamaker constant for very thin liquid films has had a considerable experimental development while understanding the influence of the contact line region in boiling mechanisms [12–15].

1.3. The critical micelle concentration, CMC, and surfactants in aqueous solutions

The CMC is the concentration of the surfactant monomer that initiates the formation of aggregates (association colloids) and remains unchanged in the solution even for increasing concentrations of the surfactant. The hydrocarbon interior of aggregate structures as spherical micelles share the hydrophobic endings of the amphiphilic molecules while their hydrophilic head-group occupies the aggregate's surface area for minimization of the mean interaction free energy. The CMC concentration also represents the value that produces a stable micelle state for adequate aqueous solution conditions (electrolyte concentration or pH) [2].

Increasing the concentration of a surfactant in solution is possible to determine the CMC of the mixture as the one that first reaches the lowest value of θ. Concentrations of the surfactant greater than the CMC do not decrease further the value of θ, while the addition of a poly-ionic salt (high ionic strength) causes its increase.

Gurkov et al. [16] investigated the influence of surfactants on heat exchange systems finding that the rupture of an extremely thin layer of the surfactant on the solid initiates the evaporation. The changes of interfacial tension on the solid cause a Marangoni effect that produces an oscillatory disturbance on supposed spherical bubbles of the boiling liquid. Waserkar [17] offered a complete evaluation of the effect of anionic and cationic surfactants on h, and reached the conclusion that its highest value occurs close to the CMC. Zhang and Manglik [18] observed that the CMC of cetyl–trimethylammonium–bromide (CTAB) occurred at 400 ppm, and that the increase of h depends on the molecular weight of the surfactant and its ionic charge. Tzan and Yang [19] performed a series of boiling experiments adding sodium–lauryl–sulfate (SLS) to water in the range of 0 to 1500 ppm. h increased for concentrations from 100 to 700 ppm because the surfactant reduced the tendency of the bubbles to coalesce, and increased their number; h decreased above 700 ppm. Yang and Maa [20] demonstrated that the addition of surfactants SLS and SLBS (sodium–lauryl benzyl–sulfate) caused an increase of 100 to 200% in h, over the values obtained for water, because the surfactant reduced the interfacial tension and promoted the heater's wetting.

1.4. Porous coverings for increasing heat transfer coefficients

Liter and Kaviany [21] enhanced the pool-boiling critical-heat-flux (CHF) of pentane on a tube with a modulated porous-layer coating. The CHF was related to a hydrodynamic and viscous-drag liquid-choking limit inside the artery-evaporator porous structures. Further enhancement in the CHF could be accomplished reducing the modulation wavelength associated to the boiling crisis by reducing the particle size in the coating. Brautsch and Kew [22] studied the boiling and wicking limits in uniform wire mesh wicks. When vapor bubbles are trapped in the structure of the wick at high heat fluxes, they reduce the capillary pumping and the cross sectional area for flow.

The best combination of shape, orientation, material, porosity or cavities of the heating surface combined with the composition of the fluid can increase the boiling heat transfer [23]. Melendez and Reyes [24] tested porous coverings that were a good option to increase the heat transfer coefficient in the individual bubble and slug regime. The pumping of liquid towards the heater (increased wettability) and the vapor release in small bubbles from inside the coverings (not working as extended surfaces) accomplished the increment in h. The model for Darcy's vapor displacement from straight pores inside the coverings explained the controlling stage in the boiling mechanism that depends on the porosity and permeability of the covering.

This study relates the values of h in pool boiling to (a) the wettability promoted by surfactants and mixture composition; (b) the micelle states developed around small departing bubbles; and (c) the porous coverings capability for releasing small vapor bubbles. The methodology searches the description of these stages in the mechanism for pool boiling heat transfer and alternatives for increasing the heat flux (or the convective heat transfer coefficient): (a) through surface energies effects and/or (b) through the mechanical breakage of the vapor produced.

2. Experimental apparatus and procedures

The experimental set up for the evaluation of the sessile drop contact angle was developed in our laboratory, and constructed according to the progress in the reduction of measurement's standard deviation or experimental error. The experimental set up for contact angle measurement consisted of interchangeable metallic bases, a calibrated micropipette for depositing the sessile drop, illumination for ensuring sharp images, and an analog camera coupled to an image digitalization system. The equilibrium contact angle was measured from the digitalized image of sessile drops using Photoshop resources.

The acceptable standard deviation and reliability of the measured sessile drop contact angle was achieved under specified conditions for image digitalization. The amount of the contact angle repetitions was selected to ensure acceptable confidence levels of the measurements and the effective reduction of the experimental error. Table 1 has the probe liquids used in the

Table 1
Interfacial free energies (mJ m^{-2}) of liquids used for contact angle measurements

Liquid; CAS number	σ_{lv}	σ^D	σ^P
Formamide; 75-12-7	58.3	32.3	26.0
Glycerol; 56-81-5	64.0	34.0	30.0
Ethylene glycol; 107-211	48.0	29.0	19.0
Dimethylformamide; 68-12-2	37.3	32.4	4.9

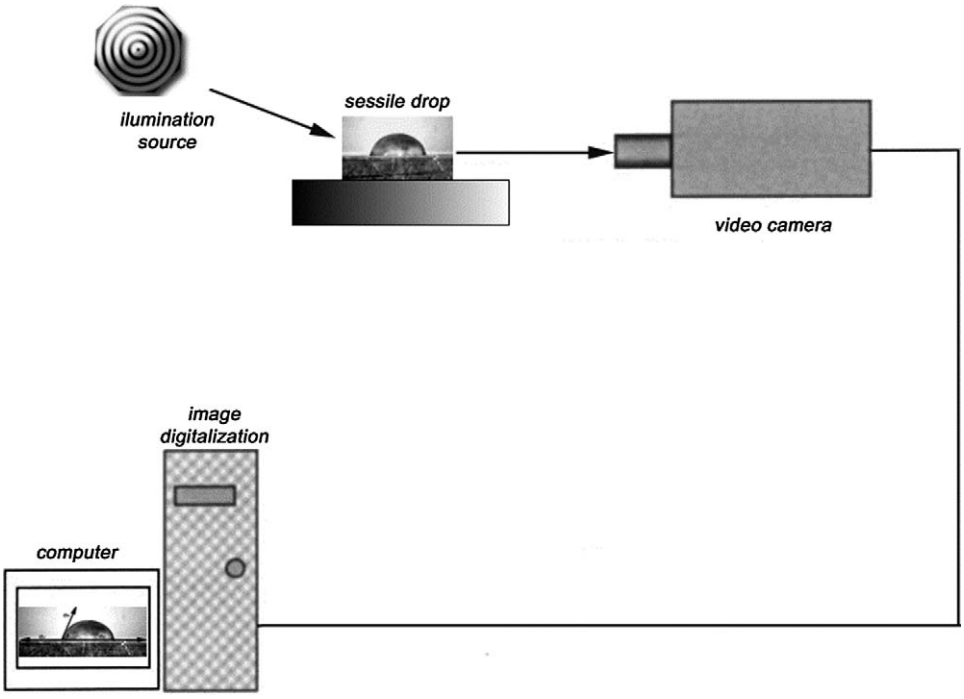

Fig. 1. Experimental set up used for contact angle measurements (goniometer).

evaluation of the measurements' statistical distribution and of some surface energies.

The average of ten independent measurements with these liquids produced the value of contact angles used in the linear model for the evaluation of the solid's surface energy, Eq. (4). This equation relies on the statistical quality of the contact angle measurements, but the linear regression analysis of the average contact angles further reduces the error of the calculated values of surface energies. The calculation of the surface energies on different metals and metallic stripes includes the statistical description of the quality of the fit.

The changes in the contact angle alone allowed the evaluation of changes in the wettability of the system. Contact angle measurements were performed on ethanol–water mixtures, on water with a surfactant, and on solutions of tri-poly-phosphate (TPP), both added up to 500 ppm. The solutions prepared in our laboratory used demineralized water, pure ethanol, the surfactant sodium lauryl sulfate (SLS), and TPP. Fig. 1 shows the goniometer employed.

The methodology described by Melendez and Reyes [24] was used for the measurement of the convective heat transfer coefficient, h; Fig. 2 shows the experimental set up. The cylindrical heating element was 6.5 mm in diameter with a length of 260 mm, and was used alone or surrounded by the porous coverings made of compacted iron wool or sinterized brass foils obtained from lathe machining. The heater, with regulated power, operated with a maximum of 1000 W. The boiling chamber had two glass sides that allowed the observation of the bubbles diameters and frequency of departure.

Measuring the number of pores per external surface area and average pore diameter of the coverings from surface photographs were calculated their porosity and permeability from a straight tube model [23]

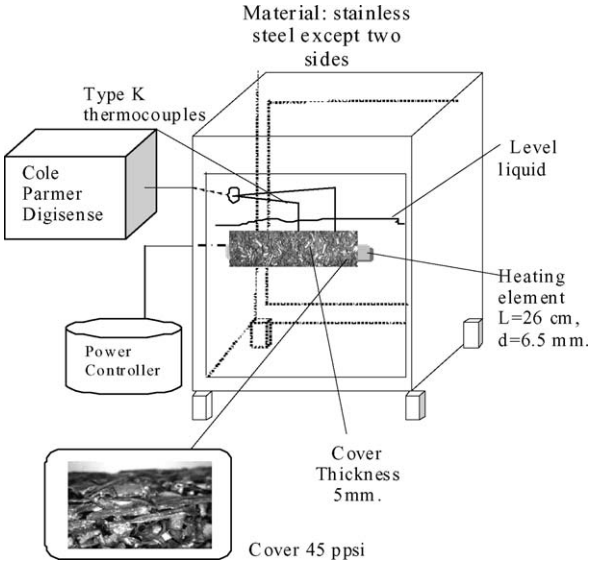

Fig. 2. Pool boiling chamber used for capturing the boiling characteristics. The horizontal heating element crosses the image with thermocouples attached.

$$\text{Unit volume of covering} = 3N^2\frac{\pi d_p^2}{4}t = (1-\varepsilon)t^3 \tag{5}$$

$$\text{Permeability} = K = \frac{\varepsilon d_p^2}{32} \tag{6}$$

The description of the seven coverings used is presented in Table 2.

Table 2
Description of the coverings fabricated for these experiments

Number	Material	Pores per square inch	Pore diameter, mm	Thickness, mm	Porosity, ε	Permeability, $m^2 \times 10^9$
C_0	Heater's surface					
C_1	Compacted iron wool	50	0.4	4.203	0.960	4.800
C_2	Compacted stainless steel wool	48	0.5	2.933	0.972	7.500
C_3	Sinterized metal foils retained on mesh 10	45	0.8	5	0.817	16.332
C_4	Sinterized metal foils retained on mesh 10	45	0.8	7.25	0.614	12.228
C_5	Sinterized metal foils retained on mesh 6	30	1.2	7.25	0.614	27.647
C_6	Sinterized metal foils retained on mesh 18	50	0.5	7.25	0.642	5.0179
C_7	Sinterized metal foils retained on mesh 18	50	0.5	9.0	0.713	5.5736

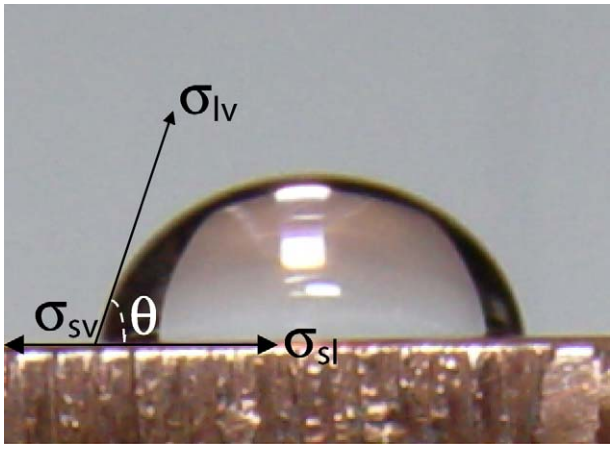

Fig. 3. Equilibrium contact angle image for glycerol on clean brass.

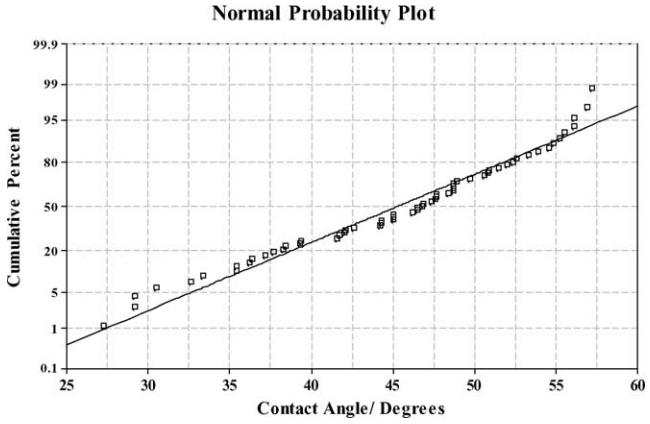

Fig. 4. Normal probability plot of the data set for the analysis of the validity of the contact angle measurements.

3. Results

3.1. Sessile drop contact angle and normal distribution assessment

The digitalized image with Photoshop enhancement, Fig. 3, provided the value of the equilibrium contact angle. Fig. 4 shows the normal distribution test performed on sixty contact angle measurements (on different systems including different base metals, bared o covered with grease, and different liquids) covering the range of contact angle values in all the experiments performed. The standard deviation associated to this test dictated ten independent measurements for ensuring the validity of each sessile drop contact angle. The standard deviation of the sets of repetitions is below 3% of the measured values.

3.2. Surface energy of metals

Using the four liquids of Table 1, and the regression analysis on sets of data shown in Fig. 5, the values of surface energies obtained for tin, copper, brass and brass metal foils are shown in Table 3. These calculations tested the experimental procedures for evaluation of the contact angles and the validity of the correlation for the calculation of surface energies, Eq. (4). These results show that the surfaces of tin and copper cleaned with acetone have surface energies of approximately 60 mJ m^{-2}. The surfaces of these metals covered with oil or grease reduced their surface energy to about 40 mJ m^{-2}. Brass

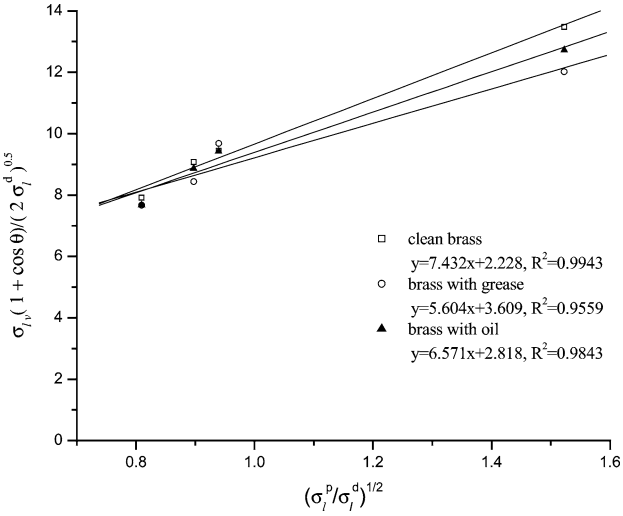

Fig. 5. Solid's surface free energy calculations with regression analysis (only the coefficient of determination, R^2, is shown).

surface had surface energies of about 40 mJ m^{-2} and remained unchanged by the cleaning procedure. The brass metal foils used for the coverings fabrication had surface energy originally of only 40 mJ m^{-2} that were reduced to almost 20 mJ m^{-2} when covered with oil; these surface energy values characterize low energy surfaces. Thus, enhancing the wettability of the porous coverings requires the increasing of the interfacial energy of the liquid, σ_{lv}, for reducing the value of the contact angle according to Eq. (3).

Table 3
Experimentally measured surface free energies of clean and contaminated metallic surfaces

Material	σ_{ss}, mJ m^{-2}
Clean tin	62.45
Tin covered with grease	45.91
Tin covered with oil	42.76
Clean copper	60.21
Copper covered with grease	44.44
Copper covered with oil	51.12
Clean brass	45.07
Brass covered with grease	41.09
Brass covered with oil	41.48
Clean metal foils	44.78
Metal foils with grease	19.32

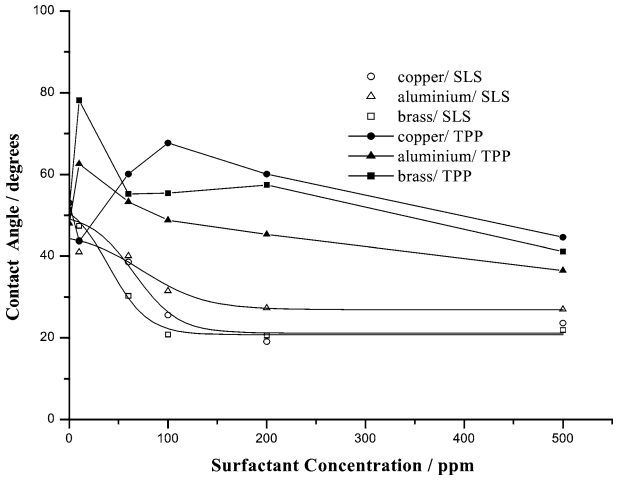

Fig. 6. Contact angle measurements for aqueous solutions of SLS and TPP.

3.3. CMC of SLS in water

Fig. 6 shows the inflexion of θ values, representative of the CMC, found at 100 ppm of SLS. There was no influence of the metallic surface used for the measurements of θ under normal laboratory conditions as can be seen on the sets of data obtained on different metals.

Contrasting the effect of the surfactant, the addition of TPP increased the value of the equilibrium contact angle and reduced the wettability of the system. The increment on θ is the highest at concentrations close to 100 ppm but disappears at higher concentrations. The concentration of TPP defines the ionic strength that could cancel the CMC effect of the aqueous solutions and their wettability. Any salt added to water would have a similar behavior, reducing the system wettability. Therefore, the basis for mixture formulation should be demineralized water with neutral pH.

3.4. CMC of ethanol–water mixtures

The evaluation of the changes in the contact angle of ethanol–water mixtures showed that at the reported concentration with the highest h value for boiling conditions below

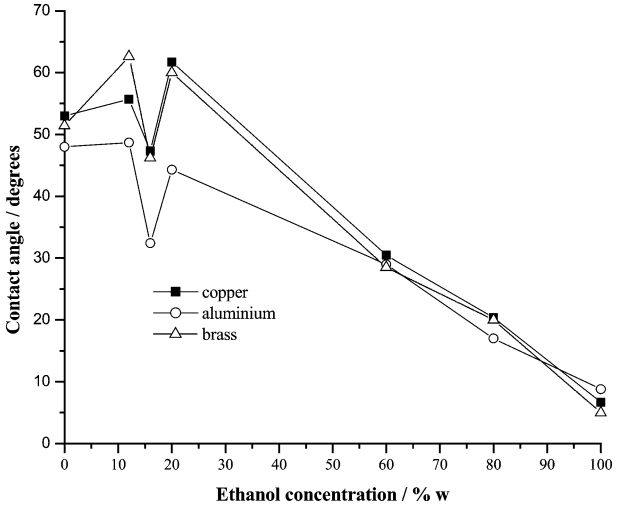

Fig. 7. Contact angle for ethanol–water mixtures on three metallic plates.

the critical heat flux [23], and with the highest critical heat flux [25,26] a CMC condition is observed. The analysis of average bubble diameters leaving a heater's surface for aqueous-ethanol mixtures showed that the minimum diameter occurred for boiling the solution with 16% by weight ethanol [23]. The increase in the wettability of the system, associated to the decrease in the value of the equilibrium contact angle, Fig. 7, occurs for solutions with 16% ethanol by weight that represents also a CMC for ethanol as a surfactant. The behavior of the hydrated states of ethanol at this composition show a hydrophobic side directed towards the vapor–liquid interface, and the corresponding hydrophilic ends that tend to minimize the micelle-structure surface-area. Thus, the increase in values of h for the mixture with 16% ethanol reflects the surface active behavior of ethanol as (a) a non-ionic surfactant at its CMC that reduces the size of departing bubbles (as spherical micelle geometries) facilitating their release; and (b) as a solution of increased wettability supplying more liquid to the active nucleation sites on the heater.

3.5. Influence of porous covering on h

The influence of the porous covering alone on the values of h was assessed boiling water, Fig. 8. The coverings C_3 to C_7 increased the values of h over the values obtained with the uncovered heater, C_0. These coverings were made with metal foils obtained from lathe machining and classified through sieving before sinterization at 800 °C. C_3 produced the highest values of h with the lowest ΔT values, resulting from its thickness (5 mm) being the lowest in this set of experiments. The other coverings tested, C_4 to C_7, generated very similar values of h and excess temperatures.

The porosity (ε) defines the behavior of the coverings for enhancing boiling heat transfer. ε increases for higher surface pore numbers and lower thicknesses. This combination reflects that the vapor release breaking the bubbles through the cover-

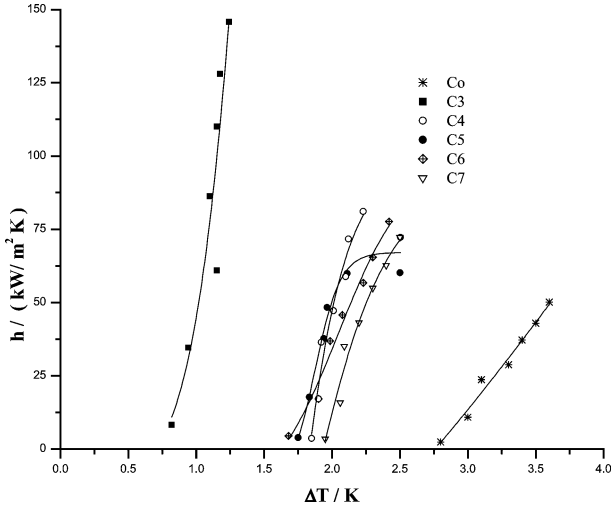

Fig. 8. Effect of the average pore diameter of the heater's cover on the values of h for boiling water.

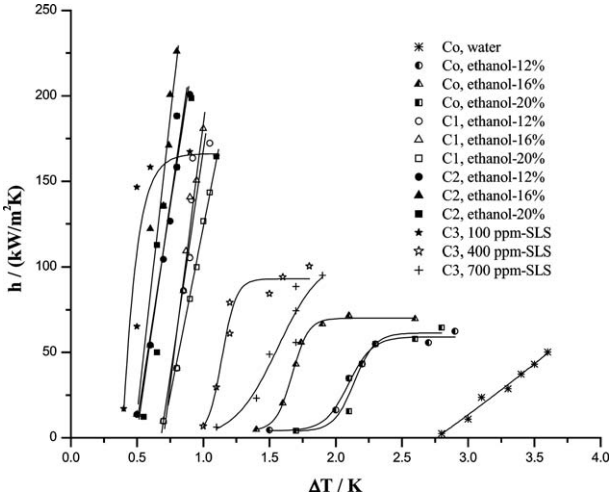

Fig. 9. Pool boiling heat transfer coefficients measured with water, 100 and 400 ppm SLS aqueous solutions, 16% by weight ethanol aqueous solution, and with covered and bare heater (the porous covering C_3).

ing controls the heat flux and h. C_3 had the highest porosity calculated by Eq. (7), Table 2, of the group C_3 to C_7

$$\varepsilon = 1 - 3N^2 \frac{\pi}{4}\left(\frac{d_p}{t}\right)^2 \tag{7}$$

The values of h provide here the description of pool boiling enhancement but they can be exchanged for the more conventional relation of the surface superheat to the heat flux:

$$\frac{q}{A} = h(T_{\text{wall}} - T_{\text{saturation}}) \tag{8}$$

This expression of the results arises from the fact that geometry and solution effects are normally correlated to h.

3.6. Influence of porous coverings and the CMC of the aqueous solutions on h

Fig. 9 shows the values of h obtained with the combinations of conditions that reflect the influence of wettability and covering porosity on pool boiling. Coverings C_1 and C_2, made of iron wool, and C_3 described above, were compared against the results of boiling mixtures on the uncovered heater, C_0. The highest values of h were obtained with the combination of the porous covering C_2, and the solution containing 16% ethanol. C_1 produced smaller h values, although its highest values with the 16% ethanol mixture. In this covering the pore diameter was too small and the covering thickness high, retarding the vapor release. C_3 produced even smaller h values due to its thickness greater than those of C_2 and C_1 and the difference in the geometry of the channels formed by the materials.

From Darcy's law,

$$\frac{\mathrm{d}P}{\mathrm{d}y} = \frac{\mu_v}{K} V \tag{9}$$

the vapor flow in straight pores can be calculated combining Eqs. (5), (6) and (9):

$$\overset{o}{m} = \frac{\pi}{128}\left(\frac{\rho_v \sigma_{lv}}{\mu_v}\right)\left(\frac{\varepsilon d_p^3}{t}\right) = \frac{\pi}{4}\left(\frac{\rho_v \sigma_{lv}}{\mu_v}\right) K \frac{d_p}{t} \tag{10}$$

The enhanced heat transfer in the coverings, Fig. 9, is controlled by the vapor release, and Eq. (10) explains these results. The vapor flow escaping from the porous covering is proportional to the average pore diameter (K is proportional to d_p^2) and inversely proportional to the covering thickness. The average pore diameter does not seem to control the pressure drop because coverings C_1 and C_2 had values almost half the value of C_3. Because of its thickness, covering C_3 had the highest vapor pressure drop and produced lower h values.

The lines for h of the mixtures on C_0 and on C_3 in Fig. 9 have a constant plateau of the h values. This plateau implies the presence of a resistance to vapor escape as explained by Eq. (10). For C_3 this plateau is present in the three experimental data sets shown. The use of the surfactant at the CMC (100 ppm) reduces the resistance to vapor flow in the covering by reducing the bubbles diameter and preventing their coalescence. C_3 generated the highest h values with the lowest ΔT in these conditions. Increasing the concentration of the surfactant SLS to 400 and 700 ppm reduced the micelle formation in the departing bubbles and the values of h. The excess surfactant breaks the equilibrium state of spheric micelles minimizing the surface energy and area. The increment in the ionic strength (associated to the higher concentration of the surfactant) reduced the wettability, as explained in Fig. 6, and the resultant effect is a lower capacity for releasing the vapor flow.

The same sigmoid description of the values of h was obtained on the heater with no covering. Over the uncovered heater the departing bubbles coalesce and limit their release; the ethanol aqueous solutions boil in these conditions with lower excess temperature and produce higher values of h than the boiling of water. Although there is an increment in h with solutions of 12 and 20% over the boiling of water, the highest h value is for the solution with 16% ethanol.

Fig. 9 comprises the augmentation in heat transfer derived from the use of the porous covering, the binary mixture, and the presence of a surfactant. For the coverings that had only linear behavior in the range of heat transfer tested it is expected that

they could reach the sigmoid functionality between ΔT and h at higher heat transferred. Eventually, the porous media used for mechanically breaking the departing bubbles from the heater would have the restriction of pressure drop on vapor flow.

4. Conclusions

The sessile-drop contact-angle technique is apt for in situ evaluation of the boiling system wettability that modifies the boiling behavior of a mixture.

The use of statistical concepts improves the calculations of the boiling system wettability from drop measurements. The size of the sample and the linear regression analysis of the average equilibrium-contact-angles reduce the dispersion of the results.

The increase in h values corresponds to the increase of the wettability of the solid–liquid boiling system. The wettability of the system increases with decreasing contact angle. This effect is maximized at 16% ethanol by weight in water, or with the addition of a maximum of 100 ppm of SLS to water.

The mixture composition and the use of surfactants reflect that the vapor bubble formation is related to spherical micelles with minimum surface area from the equilibrium of hydrophilic forces. The result is the formation of stable bubbles with low diameters.

The porous coverings enhance boiling heat transfer through vapor–bubble size-reduction when the size and shape of the pores, and covering thickness handle the vapor flow without pressure drop restriction.

The porous cover could increase the values of h but its design (thickness and pores per square inch) should be balanced to maximize results, as the case of C_2 among the coverings constructed.

The vapor release from the porous covering is the limiting step for boiling of a mixture in a porous covering. The vapor release rate could be increased by the mixture composition, the addition of a surfactant at its CMC, or the use of a porous covering that together reduce the bubbles' diameter and their coalescence. These variables have a synergistic effect on the enhancing of pool boiling heat transfer.

References

[1] R. Reyes, P.C. Wayner Jr, An adsorption model for the superheat at the critical heat flux, Trans. ASME J. Heat Transfer 117 (1995) 779–782.
[2] J.N. Israelachvili, Intermolecular and Surface Forces, Academic Press, New York, 1985.
[3] F. Fowkes, Attractive forces at interfaces, Ind. Engrg. Chem. 56 (1964) 40–52.
[4] F. Fowkes, Wetting, Soc. Chem. Ind. Monograph, vol. 25, London, 1967, p. 3.
[5] J. Lyklema, The surface tension of pure liquids. Thermodynamic components and corresponding states, Colloids Surfaces A: Physicochem. Engrg. Aspects 156 (1999) 413–421.
[6] E. Chibowski, R. Perea-Carpio, Problems of contact angle and solid surface free energy determination, Adv. Colloid Interface Sci. 98 (2002) 245–264.
[7] F. Fowkes, Dispersion force contributions to surface and interfacial tension, contact angles, and heats of immersion, contact angle, wettability, and adhesion, Adv. Chem. 43 (1964) 99–111.
[8] W.A. Zisman, Relation of the equilibrium contact angle to liquid and solid constitution, Adv. Chem. Ser. (1964) 1–51.
[9] M. Mantel, J.P. Wightman, Influence of the surface chemistry on the wettability of stainless steel, Surface Interface Anal. 21 (1994) 595–605.
[10] R. Reyes, P.C. Wayner Jr, Interfacial models for the critical heat flux superheat of a binary mixture, in: Proceedings of the 32nd National Heat Transfer Conference, 1997, 342, pp. 187–194.
[11] R. Reyes, P.C. Wayner Jr, A Kelvin–Clapeyron adsorption model for spreading on a heated plate, Trans. ASME J. Heat Transfer 118 (1996) 822–830.
[12] M. Potash, P.C. Wayner Jr, Evaporation from a two-dimensional extended meniscus, Internat. J. Heat Mass Transfer 15 (1972) 1851–1963.
[13] B.V. Derjaguin, N.V. Churaev, Structure of water in thin layers, Langmuir 3 (1987) 607–612.
[14] B.V. Derjaguin, N.V. Churaev, Ya.I. Rabinovich, The modern state of the macroscopic theory of molecular forces and the results of its experimental verification for thin interlayers, Adv. Colloid Interface Sci. 28 (1988) 197–244.
[15] S. DasGupta, J. Schonberg, I.Y. Kim, P.C. Wayner Jr, Use of the augmented Youg–Laplace equation to model equilibrium and evaporating extended menisci, J. Colloid Interface Sci. 157 (1993) 332–342.
[16] T. Gurkov, K. Danov, N. Alleborn, H. Raszillier, F. Durst, Role of surface force in the stability of evaporating thin liquid films that contain surfactant micelles, J. Colloid Interface Sci. 198 (1998) 224–240.
[17] V.M. Waserkar, Nucleate pool boiling heat transfer in aqueous surfactant solutions, PhD thesis, University of Cincinnati, 2001.
[18] J. Zhang, R. Manglik, Pool boiling heat transfer in aqueous solutions of a cationic surfactant, in: Proceedings of the 6th ASME–JSME Thermal Engineering Joint Conference, March 16–20, 2003, TED-AJ.03-248.
[19] Y.L. Tzan, Y.M. Yang, Experimental study of surfactant effects on pool boiling heat transfer, Trans. ASME J. Heat Transfer 112 (1990) 207–212.
[20] Y.M. Yang, Y.L. Maa, On the criteria of nucleate pool boiling enhancement by surfactant addition to water, Trans. IChemE 79 (2001) 409–415.
[21] S. Liter, M. Kaviany, Pool-boiling CHF enhancement by modulated porous-layer coating: theory and experiment, Internat. J. Heat Mass Transfer 44 (2001) 4287–4311.
[22] A. Brautsch, P.A. Kew, Examination and visualization of heat transfer processes during evaporation in capillary porous structures, Appl. Thermal Engrg. 22 (2002) 815–824.
[23] M. Kaviany, Principles of Heat Transfer in Porous Media, second ed., Springer, Berlin, 1995.
[24] E. Melendez, R. Reyes, The pool boiling heat transfer enhancement from experiments with binary mixtures and porous heating covers, Experimental Thermal Fluid Sci., in press.
[25] C.F. Bonilla, C.W. Perry, Heat transmission to boiling binary liquid mixtures, AICHE (1941) 685–705.
[26] S. Van Stralen, R. Cole, Boiling Phenomena: Physicochemical and Engineering Fundamentals and Applications, Hemisphere, Washington DC, 1979 (Chapter 2).